Edinburgh Research Explorer

Wave-Induced Breaking and Wave Set-up Representation by Coupling Spectral Wave and Coastal Hydrodynamics Models

Depth-Induced Breaking and Wave Set-up Representation by Coupling Spectral Wave and Coastal Hydrodynamics Models

Anastasia K. Fragkou[1], Athanasios Angeloudis[2], Vengatesan Venugopal[3] and Christopher Old[4]

[1,2,3,4] School of EngineeringUniversity of Edinburgh, Edinburgh, UK
email : A.Fragkou@ed.ac.uk
email : A.Angeloudis@ed.ac.uk

Abstract

A parallelised coupled two-dimensional model is developed to capture wave-current interactions at regional scales. The framework comprises of a spectral wave model, Simulating WAves Nearshore (SWAN), and a coastal hydrodynamics shallow-water equation model, *Thetis*. The two models are coupled through the Basic Model Interface (BMI) structure. They run iteratively and exchange information at prescribed time-intervals. SWAN provides the necessary parameters for the calculation of radiation stress, introduced in Thetis, upon solving the action density equation in a manner encompassing source terms accounting for deep- and shallow-water phenomena. In turn, Thetis returns water elevation and current velocity fields by considering the 2-D depth-averaged formulation of the shallow water equations. The coupled model's capability to account for depth-induced breaking, wave set-up and bed friction is tested using the physical modelling experiment of Boers (1997) on the behaviour of waves acting on a barred beach. The model's results exhibit good correlation with experimental data, which consists of derived wave characteristics and water elevation measurements. Additionally, the model's performance is compared against other coupled models with 3-D ocean model. The proposed model's results showcase the same level of accuracy as other coupled models and could be extensible to 3-D modelling applications and complex geometries

Keywords: Wave-current interactions; Depth-induced breaking and wave-setup; Shallow-water equations; Spectral wave modelling; Coupled model

1. INTRODUCTION

The phenomenon of wave-current interactions is crucial at coastal areas, as surface gravity waves and tidal currents are often encountered simultaneously. Their concurring presence affects each other; the wave transformation processes generate radiation stress and are influenced by the water levels and the presence of currents. Radiation stress in turn affects currents and water setup, compounded by bottom friction and vertical mixing. The accurate representation of such interactions is motivated by a plethora of applications and phenomena, such as the evolution of coastal morphology due to sediment transport (Santos et al., 2009), scouring around offshore structures (Zhang et al., 2021), mixing of pollutants nearshore (Zhang et al., 2021), design of offshore and coastal infrastructure, impacts of marine energy projects (Santos et al., 2009); and storm surges (Brown, 2010).

The coupling of ocean models with wave models originated by the need to study such interactions. Some of the existing coupled models are: (i) COAWST (Warner et al., 2010), which combined the curvilinear 3-D ocean model Regional Ocean Modeling System (ROMS; Moore et al., 2011) with the spectral wave model Simulating WAves Nearshore (SWAN; Booij et al., 1999); (ii) the coupled model described in Dietrich et al. (2011), which combines the 3-D shallow water model ADCIRC (Westerink et al., 2008) with the spectral wave model SWAN; (iii) the 3-D current model SELFE (Zhang & Baptista, 2008) coupled with the spectral wind wave model WWM-II (Roland, 2009) described in Roland et al. (2012); and (iv) the work of Marsooli et al. (2017) combining the Stevens Institute of Technology Estuarine and Coastal Ocean Model (sECOM; Marsooli et al., 2016) with the Mellor-Donelan-Oey (Mellor et al., 2008) wave model. A common characteristic of the aforementioned models is three-dimensionality of their ocean model and the adoption of an explicit numerical scheme inducing considerable computational costs. Additionally, many models in the literature are not validated against experimental data and/or analytical solutions.

In this work we present a new parallelised multiscale coupled model, which links integrally the 2-D formulation of the depth-averaged shallow-water equations model, *Thetis* (Kärnä et al., 2018), with the spectral wave model SWAN. The novelty of this approach is that a parallel 2-D shallow-water equation model, which utilizes a semi-implicit numerical scheme, is applied. Intrinsically, these characteristics lead to diminished computational times, while the numerical scheme supports larger timesteps compared to the other

models. The experimental setup of Boers (1997) is used to validate the model's accuracy to capture wave-induced setup and depth-induced wave-breaking, alongside friction. The model's results are compared against the experimental data of Boers, as well as the results provided by the coupled model of Roland et al. (2012) and Marsooli et al. (2017) that considered the same study.

2. METHODS

2.1 Spectral Wave Model (SWAN)

The spectral wave model SWAN solves the action density equation to calculate wave characteristics and spectra

$$\frac{\partial N}{\partial t} + \nabla_{x,y} \cdot (\boldsymbol{c_{xy}} N) + \nabla_{\sigma,\theta} \cdot (\boldsymbol{c_{\sigma,\theta}} N) = \frac{1}{\sigma} \sum S \qquad [1]$$

with

$$\sum S = S_{in} + S_{ds} + S_{nl} + S_{bf} + S_{brk} \qquad [2]$$

where the first LHS term of Eq. [1] denotes the changes of action density N in time t, while the second term expresses its advection in the geographical domain with propagation speed $\boldsymbol{c_{xy}}$. The third term represents the shifting of frequencies in the frequency (σ) domain and the refraction in the wave direction (θ) domain with propagation speed $\boldsymbol{c_{\sigma,\theta}}$. The RHS of Eq. [1] comprises the sum of the source and sink terms (Eq. [2]), which include the wind input (S_{in}), whitecapping dissipation (S_{ds}), non-linear wave-wave interactions (S_{nl}), bottom friction (S_{bf}) and depth-induced wave-breaking (S_{brk}) effects [see Booij et al. (1999) for details]. A first-order semi-Lagrangian scheme, called Backward Space Backward Time (BSBT), is employed for propagating in time and space.

2.2 Ocean Model *Thetis*

Thetis, a 2-D/3-D coastal model, employs the Firedrake finite element modelling framework, which uses abstraction for the description of the weak formulation of PDEs and the generation of automated code (Rathgeber et al., 2016). It considers the non-conservative formulation of the shallow water equations accounting for wetting and dying by utilizing the formulation of Kärnä et al. (2011)

$$\frac{\partial \eta}{\partial t} + \frac{\partial \tilde{h}}{\partial \mathrm{t}} + \nabla \cdot (\tilde{H} \boldsymbol{u}) = 0 \qquad [3]$$

$$\frac{\partial \boldsymbol{u}}{\partial t} + \boldsymbol{u} \cdot \nabla \boldsymbol{u} + g \nabla \eta = \nabla \cdot (\nu (\nabla \boldsymbol{u} + \nabla \boldsymbol{u}^T)) - \frac{\boldsymbol{\tau_b}}{\rho \tilde{H}} - \frac{\boldsymbol{\tau_W}}{\rho \tilde{H}} \qquad [4]$$

where η is the water elevation; $H_d = h + \eta$ is the total water depth; $\boldsymbol{u}$ is the depth-averaged velocity vector; and ν is the kinematic viscosity of the fluid. The wetting and drying formulation introduces a modified bathymetry $\tilde{h} = h + f(H_d)$ to ensure positive water depth defined by

$$f(H_d) = \frac{1}{2} \left(\sqrt{H_d^2 - \alpha_{wd}^2} - H_d \right) \qquad [5]$$

where α_{wd} is a wetting and drying parameter with dimensions of length. Thus, the total water depth is also modified $\tilde{H} = H_d + f(H_d)$. The bed shear stress effects ($\boldsymbol{\tau_b}$) utilize the Manning formulation with a friction coefficient n_M, while the wave effects on currents are described by the term $\boldsymbol{\tau_{WEC}}$.

The shallow-water equations are discretised using the discontinuous Galerkin finite element method (DG-FEM) and the semi implicit Crank-Nicolson scheme is selected for time marching the solution. The resulting system of equations is solved iteratively by Newton's method as implemented in PETSc.

2.3 Coupling procedure

The coupling procedure commences with the initialisation of Thetis, followed by SWAN. Consecutively, SWAN and Thetis run on an iterative basis (Figure 1), exchanging information at prescribed time intervals. SWAN provides the necessary statistical wave parameters for the calculation of the radiation stress and the wave roller contribution. These parameters are the significant waveheight, H_s, the wave direction, θ_m, the

wavelength, λ, and the percentage of wave breaking, Q_b. In turn, *Thetis,* provides SWAN with water elevation, η, and current, $\mathbf{u}$, information.

The calculation of vertically integrated stress induced by wave effects, based on a modified version proposed by Mellor (2015) which accounts for the radiation stress and wave rollers, is

$$\overline{S_{ij}}^{z} = E\left[\frac{c_g}{c}\frac{k_i k_j}{k^2} + \delta_{ij}\left(\frac{c_g}{c} - \frac{1}{2}\right)\right] + E_r \frac{k_i k_j}{k^2} \qquad [6]$$

where $\overline{S_{ij}}^{z}$ = vertically integrated effects from wave to currents; E = the wave energy; c_g = group velocity; c = phase velocity; k = wavenumber, δ_{ij} = Kronecker delta function (=1 when $i = j$ or =0 otherwise), and E_r = energy due to the roller-wave interface calculated according to Duncan (1981)

$$E_r = \rho g A_r \sin\theta \qquad [7]$$

where A_r is the roller area and θ the roller angle. The first term on the RHS of Eq. [6] represents the radiation stress, while the second the roller stress. The gradient of $\overline{S_{ij}}^{z}$ describes the effects of waves on currents

$$\boldsymbol{\tau_w} = \nabla \overline{S_{ij}}^{z} \qquad [8]$$

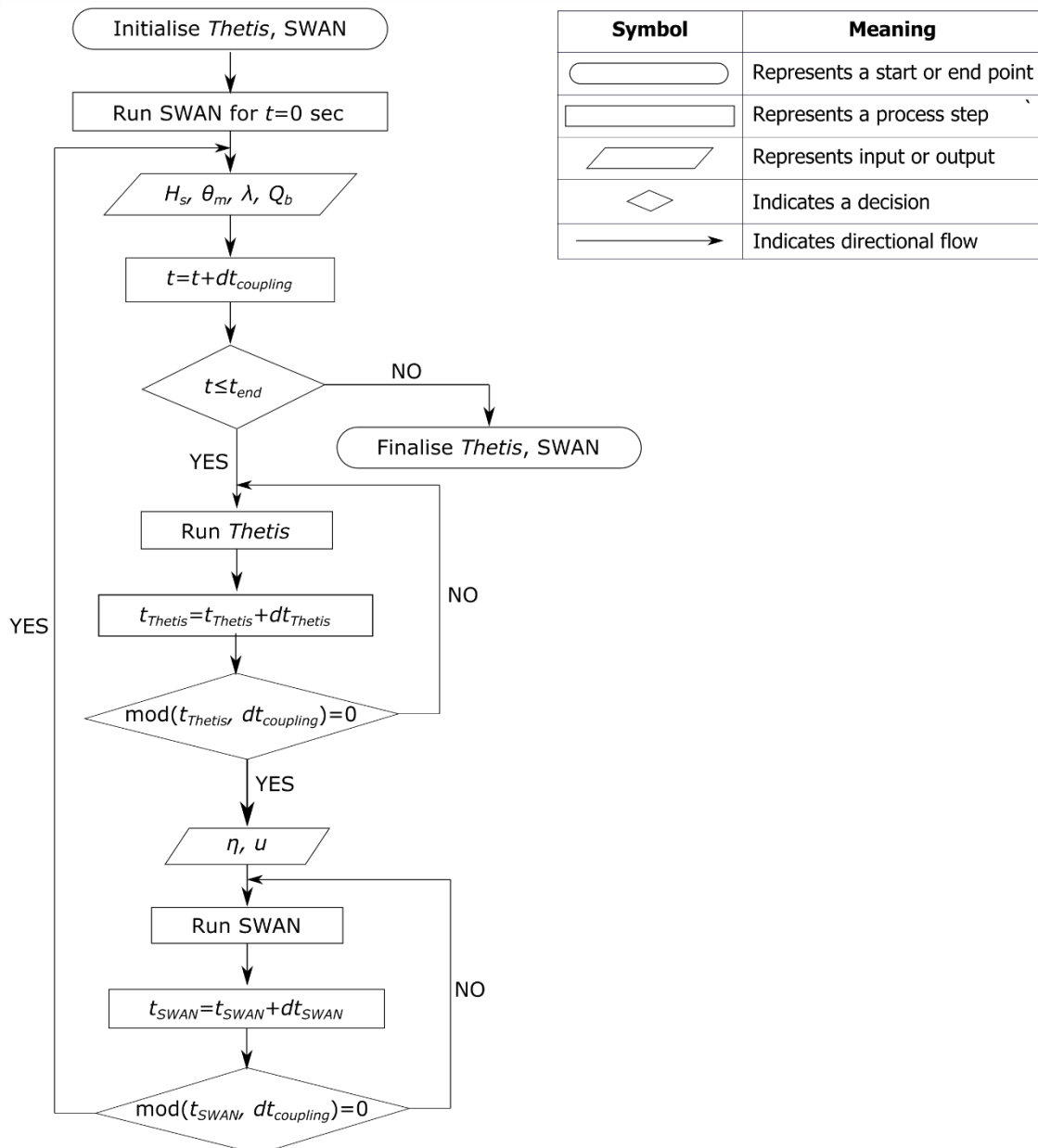| Symbol	Meaning
(rounded)	Represents a start or end point
(rectangle)	Represents a process step
(parallelogram)	Represents input or output
(diamond)	Indicates a decision
(arrow)	Indicates directional flow

Figure 1. The coupling procedure between Thetis and SWAN

The coupled model is facilitated by the Basic Modeling Interface (BMI; Hutton et al., 2020), which is a library of functions provided in several programming languages, as well as Fortran for SWAN and Python for *Thetis*. The two models have been refactored to fit into the provided BMI "template". SWAN, which is written in Fortran, is converted into a python package utilizing its BMI refactored code, a Fortran-C interoperability layer and the programming language Cython.

3. BOERS EXPERIMENT
3.1 Domain

Boers (1997) examined the phenomena of depth-induced wave breaking and wave-induced set-up under laboratory conditions. Exploiting a flume with length 40 m, width 0.8 m and height 1.08 m, they recorded the evolution of random unidirectional waves over a bar trough profile. The flume's bottom was composed of sand with a smooth concrete layer finish. Three wave conditions, described by their significant wave height H_s and their peak period T_p, were applied: (a) $H_s = 0.16$ m and $T_p = 2.1$ sec; (b) $H_s = 0.22$ m and $T_p = 2.1$ sec; and (c) $H_s = 0.10$ m and $T_p = 3.4$ sec (Table 1) with wave direction towards the shore.

Table 1. Wave conditions in the Boers experiment

Case	H_s [m]	T_p [sec]
A	0.16	2.1
B	0.22	2.1
C	0.10	3.4

The numerical domain representing the experimental setup consists of two domains: (i) the outer domain, D_1; and (ii) the nested domain D_2. The two domains share the same length of 45 m, while the former has a width of 15 m and the latter of 5 m. The bathymetry is constant in the y-direction and ranges from 0.80 m to 0.05 m in x-direction (Figure 1). The coupled model is implemented only in the area of interest D_2, while domain D_1 is only applicable for SWAN
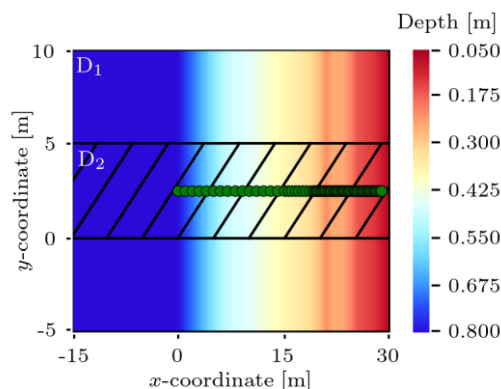

Figure 1. The numerical domain for the Boers experiment (1997) and its bathymetry. The green dots represent the locations of the experimental measurements.

The wave boundary condition is applied to the left boundary of SWAN, while the right boundary represents the shore. Domain D_1 provides the boundary conditions for the bottom and top boundaries of domain D_2. Similarly for *Thetis*, the measured water elevation is imposed in the left boundary, while a no-slip condition is applied on the right boundary depicting the shore. Finally, the top and bottom boundaries are described by a slip condition mimicking smooth surfaces typical of lab-scale experiments.

The mesh employed by SWAN is uniformly structured in both directions, while the mesh in *Thetis* is unstructured with the mesh element length being consistent in both models. Due to the semi-implicitness of *Thetis*' numerical scheme, bigger timesteps are afforded and thus, the same timestep as SWAN can be sustained. Bed friction is accounted for by employing the Madsen formulation (Madsen, et al., 1989) with its default values in SWAN and by a quadratic manning formulation in *Thetis*. Depth-induced wave breaking is considered through the bore-based model of Battjes & Janssen (1978) with rate of dissipation 2.5 and breaker index 0.48, while no wind input is accounted. Due to the small size of the domain, the model is run in one core with a simulation time of 20 min.

3.2 Sensitivity analyses

A balance between model accuracy and computational cost is pursued through several sensitivity analyses on case B (Table 1), focusing initially on SWAN and its mesh discretisation. Mesh spacing is uniform in both x- and y-directions ranging from 0.10 m to 0.40 m with no noteworthy differences in the results as the coefficient of determination is $R^2 \approx 0.97$ for all discretisations and r.m.s. error $5 \cdot 10^{-5}$ m. Following a study on

the effect of discretisation in the σ-space with resolutions between 0.25° and 2°, the value of 1° is selected due to the convergence in results. Lastly, an exploration of SWAN's timestep, which coincides in this case with both the coupling and *Thetis*' timesteps, is conducted. It is noted that for $\Delta t > 30$ sec the model diverges, thus, the timestep ranges from 2 sec to 30 sec. All values produce identical results, with differences occurring in the convergence time and the elapsed real time. The former increases almost linearly with the timestep, while the latter decreases following a power-law curve (Figure 2). Hence, a timestep of 10 sec is selected, which provides a 2.2 min wall-clock time and converges at 6 min, which is 30% of the simulation time.

The key parameter defining the water elevation in *Thetis* is the wetting and drying parameter α_{wd}. Its values, ranging from 0, i.e. no implementation of the wetting and drying formulation, to 0.5, produces a spectrum of water elevations. As depicted in Figure 3, the water elevation nearshore decreases as α_{wd} increases due to the growing downward shifting of the bathymetry. The violation of one of the shallow-water equation assumptions could contribute to this behaviour, as the mesh is of the same or smaller order compared to the water depth nearshore. Hence, the best approximation to the experimental data is achieved with $\alpha_{wd} = 0.38$.
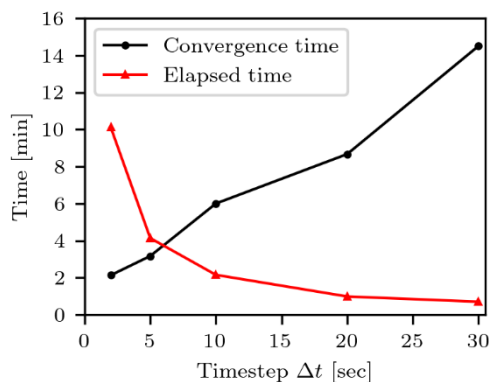

Figure 2. The elapsed and convergence time of the various timesteps during the sensitivity analysis of the timestep of SWAN when run serially
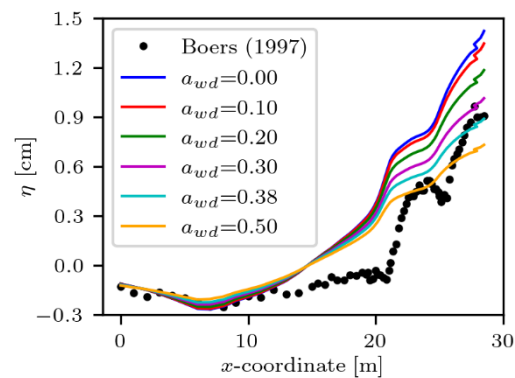

Figure 3. The water elevations for the various values of the wetting and drying parameter. The black dots represent the experimental data.

4. RESULTS

The parameters determined in the sensitivity analysis for case B, i.e. for. $H_s = 0.22$ m and $T_p = 2.1$ sec, are utilized in the other two cases. The Boers experiment was also tested by Roland et al. (2012) and Marsooli et al. (2017) for validation purposes. The former utilized all three wave conditions described in Section 3.1, while Marsooli et al. (2017) the last two (Figures 4-6)

Table 2. Coefficient of determination, root mean squared (r.m.s.) error and mean absolute (m.a.) error between the coupled models and the experimental data

		Significant Waveheight, H_s			Water elevation, η		
		R^2 [-]	r.m.s. error [m]	m.a. error [m]	R^2 [-]	r.m.s. error [cm]	m.a. error [cm]
Case A	**Roland et al. (2012)**	0.959	0.000	0.006	0.405	0.039	0.161
	Model	0.956	0.000	0.006	0.777	0.015	0.089
Case B	**Roland et al (2012)**	0.979	0.000	0.005	0.639	0.039	0.168
	Marsooli et al. (2017)	0.981	0.000	0.005	0.800	0.027	0.130
	Model	0.977	0.000	0.006	0.683	0.042	0.159
Case C	**Roland et al. (2012)**	0.782	0.000	0.009	-0.957	0.021	0.109
	Marsooli et al. (2017)	0.868	0.000	0.007	0.795	0.006	0.058
	Model	0.773	0.000	0.009	0.818	0.006	0.057

According to the coefficient of determination R^2 (Table 2), the model achieved good correlation with the experimental data regarding H_s as $0.77 \leq R^2 \leq 0.98$ with mean absolute (m.a.) error of 0.006 m, while for η the correlation ranges from $R^2 = 0.68$ to $R^2 = 0.82$ and the m.a. error between 0.057 to 0.159 cm. Compared to the other models, our predictions regarding H_s are quite similar to those of Roland et al. (2012), while for η our correlation is better (Figure 4b, 6b). Marsooli et al. (2017) achieve in general better results compared to our model, which is quite apparent on case C (Figure 6)
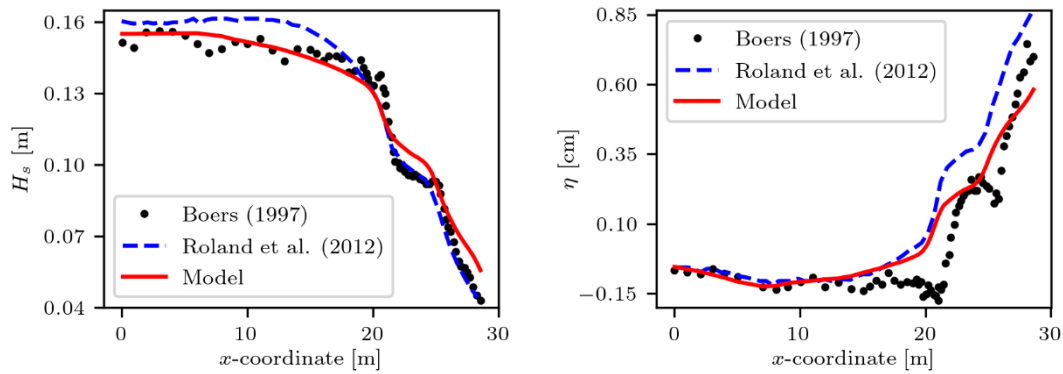
Figure 4. The significant wave height (left column) and water elevation (right column) for experimental wave condition A. The predictions of the coupled model proposed here are compared against the experimental data and the performance of Roland et al. (2012)

Figure 5. The significant wave height (left column) and water elevation (right column) for experimental wave condition B. The predictions of the coupled model proposed here are compared against the experimental data, the performance of Roland et al. (2012) and Marsooli et al. (2017)
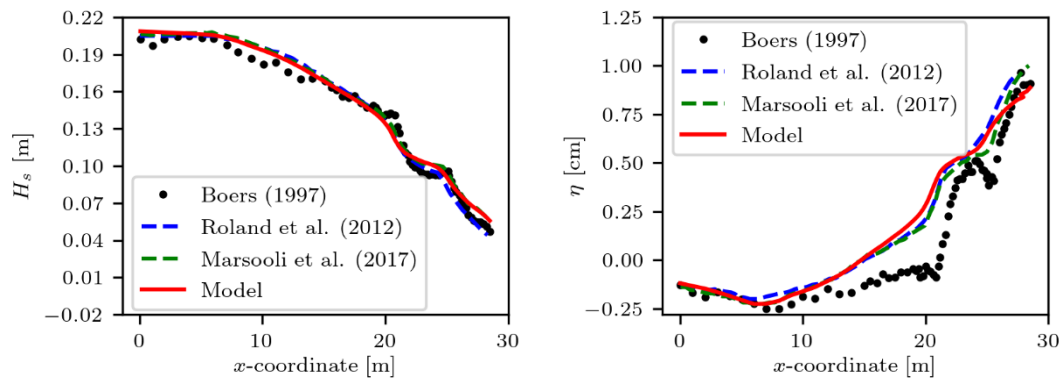

Figure 6. The significant wave height (left column) and water elevation (right column) for experimental wave condition C. The predictions of the coupled model proposed here are compared against the experimental data, the performance of Roland et al. (2012) and Marsooli et al. (2017).
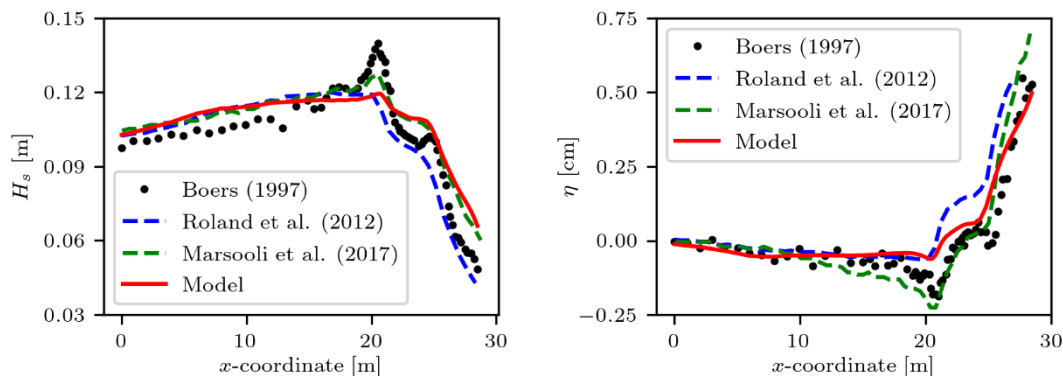
5. DISCUSSION

The coupled model presented here combines of a 2-D shallow water equation and a 2-D spectral wave model, while the models of Roland et al. (2012) and Marsooli et al. (2017) are comprised of a 3-D ocean model and a 2-D spectral wave model. Notwithstanding this difference, the performance of all models is comparable. The similar behaviour of our model and Roland et al. (2012) is ascribed to the similar wave models that utilize a JONSWAP spectrum. On the other hand, Marsooli et al. (2017) implement the spectrum of Donelan et al. (1985), which could justify the better performance of their model in the experimental wave condition C. As the forcing mechanism in this case for the ocean model is the radiation stress, better prediction of H_s will naturally lead to better prediction of the water elevation behaviour, as confirmed between our model and Marsooli et al. (2017) (Figure 6b). The better performance of Marsooli et al. (2017) model in water elevations, despite the almost identical predictions of H_s between their model and ours (Figure 5) could be attributed to their 3-D ocean model. However, despite Roland et al. (2012) also applying a 3-D ocean model, our model results in more accurate water elevations; we attribute this to the different formulation the

models adopt to calculate the radiation stress. Roland et al. (2012) utilizes the simplistic formulation of Longuet-Higgins & Stewart (1962) without accounting for wave rollers, while we employ the formulation of Mellor (2015) also including wave roller effect (Eq. [6]).

Due to the fact that the model proposed utilizes a semi-implicit scheme for the current model, we were able to use relative large timesteps compared to the other models, indicatively $\Delta t_{model} = 20\Delta t_{Roland}$ and $\Delta t_{model} = 400\Delta t_{Marsooli}$, potentially suggesting reduced wall time. In addition, our model performs similarly to Roland et al. (2012) who affirmed the robustness of their model upon convergence of both the wave and the current model to steady-state conditions.

Lastly, it was necessary to reduce the default maximum wave height to depth ratio to 0.48, a reduction of 34% compared to its default value, and increase the rate of depth-induced dissipation to 2.5 instead of 1.0, so as to not overestimate the significant wave height and accurately capture the wave breaking. A similar practice was implemented by Roland et al. (2012) as they reduced the default dissipation rate to 0.5 and increased the ratio of the maximum wave height to 0.80 instead of 0.73 to not over-dissipate the wave energy. The differences in values are likely due to the different numerics implemented by the wave models.

6. CONCLUSIONS

A new model coupling the spectral wave model SWAN with the hydrodynamics model *Thetis* to capture wave-current interactions was demonstrated. The coupling between the models is facilitated by the Basic Model Interface and the two models run sequentially. The models exchange information at prescribed time intervals and run iteratively. The model's ability to account for wave-current interactions was confirmed by employing the Boers experiment with its three wave conditions. The model predicted the significant wave height with correlation $R^2 \geq 0.77$ and the water elevation with $R^2 \geq 0.68$. Its predictions showcased the same level of accuracy as other coupled models, whose ocean model was 3-D. Thus, the ability of a 2-D ocean model coupled with a 2-D spectral wave model to accurately capture wave-current interactions at a fraction of the time utilized by the other coupled models is established.

7. ACKNOWLEDGEMENTS

8. REFERENCES

Battjes, J. A. & Janssen, J. (1978). Energy loss and set-up due to breaking of random waves. In: *Coastal engineering 1978,* 569-587.

Boers, M. (1997). Simulation of a surf zone with a barred beach; Part 1: wave heights and wave breaking. *Oceanographic Literature Review,* 4(44), p. 292.

Battjes, J.A. & Janssen, J. (1978). Energy loss and set-up due to breaking of random waves. In: *Coastal*

Booij, N., Ris, R. & Holthuijsen, L. (1999). A third-generation wave model for coastal regions: 1. Model description and validation. *Journal of geophysical research: Oceans,* 104(C4), pp. 7649-7666

Brown, J.M. (2010). A case study of combined wave and water levels under storm conditions using WAM and SWAN in a shallow water application. *Ocean Modelling,* 35(3), pp. 215-229.

Dietrich, J.C., Zijlema, M., Westerink, J.J., Holthuijsen, L.H., Dawson, C., Luettich Jr, R.A., Jensen, R.E., Smith, J.M., Stelling, G.S. and Stone, G.W (2011). Modeling hurricane waves and storm surge using integrally-coupled, scalable computations. *Coastal Engineering,* 58(1), pp. 45-65.

Donelan, M.A., Hamilton, J. & Hui, W.H. (1985). Directional spectra of wind-generated ocean waves. *hilosophical Transactions of the Royal Society of London. Series A, Mathematical and Physical Sciences,* 315(1534), pp. 509-562.

Duncan, J. (1981). An experimental investigation of breaking waves produced by a towed hydrofoil. *Proceedings of the Royal Society of London. A. Mathematical and Physical Sciences,* 377(1770), pp. 331-348.

Hutton, E.W., Piper, M.D. & Tucker, G.E. (2020). The Basic Model Interface 2.0: A standard interface for coupling numerical models in the geosciences. *Journal of Open Source Software,* 5(51), p. 2317.

Kärnä, T., De Brye, B., Gourgue, O., Lambrechts, J., Comblen, R., Legat, V. and Deleersnijder, E. (2011). A fully implicit wetting-drying method for DG-FEM shallow water models, with an application to the Scheldt Estuary. *Computer Methods in Applied Mechanics and Engineering,* 200(5-8), pp. 509-524.

Kärnä, T., Kramer, S.C., Mitchell, L., Ham, D.A., Piggott, M.D. and Baptista, A.M. (2018). Thetis coastal ocean model: discontinuous Galerkin discretization for the three-dimensional hydrostatic equations. *Geoscientific Model Development,* 11(11), pp. 4359-4382.

Longuet-Higgins, M.S. & Stewart, R. (1962). Radiation stress and mass transport in gravity waves, with application to 'surf beats'. *Journal of Fluid Mechanics,* 13(4), pp. 481-504.

Madsen, O.S., Poon, Y.K. & Graber, H.C. (1989). Spectral wave attenuation by bottom friction: Theory. In: *Coastal Engineering 1988.* pp. 492-504.

Marsooli, R., Orton, P.M., Georgas, N. & Blumberg, A.F. (2016). Three-dimensional hydrodynamic modeling of coastal flood mitigation by wetlands. *Coastal Engineering,* Volume 111, pp. 83-94.

Marsooli, R., Orton, P.M., Mellor, G., Georgas, N. and Blumberg, A.F. (2017). A coupled circulation--wave model for numerical simulation of storm tides and waves. *Journal of Atmospheric and Oceanic Technology,* 34(7), pp. 1449-1467.

Mellor, G. (2015). A combined derivation of the integrated and vertically resolved, coupled wave-current equations. *Journal of Physical Oceanography,* 45(6), pp. 1453-1463.

Mellor, G.L., Donelan, M.A. & Oey, L.Y. (2008). A surface wave model for coupling with numerical ocean circulation models. *Journal of Atmospheric and Oceanic Technology,* 25(10), pp. 1785-1807.

Moore, A.M., Arango, H.G., Broquet, G., Powell, B.S., Weaver, A.T. and Zavala-Garay, J. (2011). The Regional Ocean Modeling System (ROMS) 4-dimensional variational data assimilation systems: Part I-System overview and formulation. *Progress in Oceanography,* 91(1), pp. 34-49.

Rathgeber, F., Ham, D.A., Mitchell, L., Lange, M., Luporini, F., McRae, A.T., Bercea, G.T., Markall, G.R. and Kelly, P.H, (2016). Firedrake: automating the finite element method by composing abstractions. *ACM Transactions on Mathematical Software (TOMS),* 43(3), pp. 1-27.

Roland, A. (2009). *Development of WWM II: Spectral wave modelling on unstructured meshes.* s.l.:PhD thesis, Inst. of Hydraul. and Water Resour. Eng., Tech. Univ. Darmstadt, Germany.

Roland, A., Zhang, Y.J., Wang, H.V., Meng, Y., Teng, Y.C., Maderich, V., Brovchenko, I., Dutour-Sikiric, M. and Zanke, U. (2012). A fully coupled 3D wave-current interaction model on unstructured grids. *Journal of Geophysical Research: Oceans,* 117(C11).

Santos, J.A., Guilherme, L., Fortes, C.J., Pinheiro, L. and Simões, A. (2009). Coupling numerical models for wave propagation in the MOIA package. *Journal of Coastal Research,* Issue 56, p. 544.

Warner, J.C., Armstrong, B., He, R. & Zambon, J.B. (2010). Development of a coupled ocean-atmosphere-wave-sediment transport (COAWST) modeling system. *Ocean modelling,* 35(3), pp. 230-244.

Westerink, J.J., Luettich, R.A., Feyen, J.C., Atkinson, J.H., Dawson, C., Roberts, H.J., Powell, M.D., Dunion, J.P., Kubatko, E.J. and Pourtaheri, H. (2008). A basin-to channel-scale unstructured grid hurricane storm surge model applied to southern Louisiana. *Monthly weather review,* 136(3), pp. 833-864.

Zhang, X., Simons, R., Zheng, J. & Zhang, C. (2021). A review of the state of research on wave-current interaction in nearshore areas. *Ocean Engineering,* p. 110202.

Zhang, Y. & Baptista, A.M. (2008). SELFE: a semi-implicit Eulerian-Lagrangian finite-element model for cross-scale ocean circulation. *Ocean modelling,* 21(3-4), pp. 71-96.